Ab initio and atomistic study of ferroelectricity in copper-doped potassium niobate

Sabine Körbel* and Christian Elsässer
Fraunhofer Institute for Mechanics of Materials IWM, Wöhlerstraße 11, D-79108 Freiburg, Germany
(Received 4 March 2011; revised manuscript received 9 May 2011; published 26 July 2011)

The ferroelectric [001], [011], and [111] instabilities in $KNbO_3$ with up to 12.5 mol% Cu on K or Nb sites, respectively, are investigated using both *ab initio* density-functional theory and classical interatomic potentials. A doping level of only about 2–4 mol% Cu on K sites enhances the ferroelectric instabilities and induces a morphotropic phase boundary, while Cu on Nb sites decreases the ferroelectric energies without changing their relative order.

DOI: 10.1103/PhysRevB.84.014109 PACS number(s): 77.80.bg, 77.84.Ek, 71.15.Mb, 71.15.Nc

I. INTRODUCTION

Environment-friendly lead-free ferroelectric ceramics are currently investigated in order to substitute lead zirconate titanate [$Pb(Zi,Ti)O_3$, PZT] in future piezoelectric sensor and actuator applications. A solid solution of two or more perovskite oxides with a morphotropic phase boundary (MPB), like PZT, can exhibit enhanced piezoelectric properties.[1] The $(K,Na,Li)NbO_3$ system is a promising candidate because it has a MPB between a tetragonal phase and the orthorhombic room-temperature phase of $(K,Na)NbO_3$.[2]

With decreasing temperature, $KNbO_3$ undergoes a transition from the cubic high-temperature phase to a tetragonal one at 435 °C, to an orthorhombic one at 225 °C, and to a rhombohedral one at −10 °C (analoguous to $BaTiO_3$).[3,4] Up to a K/Na ratio of about 50%, $(K,Na)NbO_3$ undergoes the same sequence of phase transitions as $KNbO_3$.[5] The cubic phase is paraelectric, the others are ferroelectric.[4] $LiNbO_3$ crystallizes in the so-called $LiNbO_3$ structure,[6] which is perovskite related[7] and exhibits a ferroelectric instability as well. If it is forced into the perovskite structure in a solid solution with $KNbO_3$ as the other component, it stabilizes the tetragonal perovskite phase.[2,8] Because the structure of $KNbO_3$ is not tetragonal for temperatures below 225 °C, the solid solution $(Li,K)NbO_3$ has a MPB.

Because alkali niobate ceramics suffer from incomplete densification when processed using conventional techniques, sintering aids like CuO are added.[9] It is to be expected that part of the Cu is incorporated into the perovskite matrix. In a previous work,[10] we found that Cu can occupy both A or B sites in the perovskite ABO_3 structure, depending on the processing conditions. For CuO-doped $(K,Na)NbO_3$ and $KNbO_3$ produced with conventional solid-state powder processing techniques, there is strong experimental evidence that Cu substitutes for Nb (on the B site) and forms defect complexes with oxygen vacancies for charge compensation.[11,12] Nevertheless, some isolated Cu_{Nb} ions may exist in the material.

However, there is also evidence that Cu^+ and Li^+ can to some extent substitute for each other. Cu^+ and Li^+ have almost identical ionic radii.[13] Cu probably substitutes for Li in $LiNbO_3$,[14] and Li in turn substitutes for K or Na in $(K,Na)NbO_3$.[2] The structure of $CuNbO_3$ differs both from the perovskite and from the $LiNbO_3$ structure,[15] but $CuTaO_3$ is isostructural with $LiNbO_3$.[16] Although the Nb site seems to be favored by Cu, the K site should also not be ruled out as a possible substitution site for Cu in $KNbO_3$. Hence if the solid solution $(K,Cu)NbO_3$ can be produced, it can be expected to have a MPB similar to that in $(K,Na,Li)NbO_3$.

In this work, the effect of Cu on K and Nb sites on the ferroelectric instabilities in $KNbO_3$ was studied, and $KNbO_3$ doped with Cu_K was investigated for a MPB by comparing the energetical ordering of the tetragonal, orthorhombic, and rhombohedral perovskite structures as a function of the Cu content. Such an approach to find MPB's was applied, e.g., to solid solutions of $AgNbO_3$ and $PbTiO_3$, $BaZrO_3$, and $BaTiO_3$, respectively, in Ref. 17.

II. COMPUTATIONAL METHOD

The energies of the different ferroelectric phases were determined using *ab initio* density-functional theory (DFT) in the local-density approximation (LDA) and molecular statics with classical interatomic potentials.

The DFT calculations were performed using the mixed-basis pseudopotential (MBPP) method.[18–22] As in Ref. 10, *optimally smooth* norm-conserving pseudopotentials,[23] the LDA exchange-correlation functional as parametrized by Perdew and Zunger,[24] k-point meshes that are equivalent to an $8 \times 8 \times 8$ Chadi-Cohen[25] k-point mesh for the simple cubic $1 \times 1 \times 1$ unit cell, and Gaussian broadening[26] by 0.2 eV were applied.

A basis consisting of plane waves up to a maximum energy of 340 eV combined with atom-centered basis functions for K $s + p$ semicore states, O p valence states, Nb $s + p$ semicore and d valence states, and Cu d valence states was applied. The atomic positions were relaxed until the forces were smaller than 10 meV/Å. The differences in total energies between successive relaxation steps were typically of the order of 10^{-6} eV per formula unit. The ferroelectric instabilities of undoped $KNbO_3$ were determined by minimizing the total energy of a unit cell with respect to the atomic positions and the cell parameters imposing a cubic ($Pm3m$), tetragonal ($P4mm$), orthorhombic ($Amm2$), or rhombohedral symmetry, respectively. The rhombohedral structure optimization was initialized by displacing the ions in the unit cell along [111] with respect to each other. During the relaxation the structure evolved towards ($R3m$) symmetry. The cell parameters were relaxed as follows: In the cubic unit cell, only the volume was allowed to change. In the tetragonal phase, the c/a ratio was relaxed as well. The orthorhombic phase has a primitive monoclinic unit cell. Therefore in principle three

parameters (the cell volume, the monoclinic angle, and the c/a ratio) should be relaxed. In this work, in order to reduce the computational effort, the monoclinic cell angle was fixed to 90° (its experimental value is 89.74°),[4] and only the cell volume and the c/a ratio were relaxed. For comparison, the same calculations were also performed with the cell parameters fixed to the cubic ones. In the DFT supercell calculations for Cu-doped $KNbO_3$, the cell parameters were fixed to the cubic ones throughout, so that ferroelectric strain was neglected.

Cu concentrations of 12.5 and 6.25 mol% were taken into account by replacing one K or Nb atom by Cu in a simple cubic (sc, 40 atoms) and a face-centered-cubic (fcc, 80 atoms) supercell, respectively. Volume effects due to the Cu doping were considered by performing the calculations at two different volumes, the theoretical one of undoped $KNbO_3$ and the volume that minimizes the total energy of the cubic, paraelectric Cu-doped supercell. In the case of Cu_K doping, the magnitudes of the ferroelectric instabilities are almost the same for the relaxed volumes of pure and Cu_K-doped $KNbO_3$ due to the small volume change induced by Cu_K (namely 0.6% shrinkage at a doping level of 12.5 mol%). Since this volume change of the cubic supercell is rather small, in the following all calculations for Cu_K-doped $KNbO_3$ were performed at the theoretical volume of undoped $KNbO_3$. For Cu_{Nb} doping, the volume effect is stronger (about 2% expansion in the 40-atom supercell) and was therefore included in the following calculations for Cu_{Nb}-doped $KNbO_3$. In the 80-atom supercell calculations, spin polarization of the Cu ions was taken into account, while it was neglected in the 40-atom supercell calculations.

The energies of undoped and Cu_K-doped $KNbO_3$ obtained with the DFT were used to adjust a classical empirical interatomic shell-model potential (SMP) in order to determine the ferroelectric instabilities for lower Cu_K concentrations by atomistic simulation with larger supercells for which DFT calculations are unfeasibly expensive. The potential parameter set for the Cu-O interaction was obtained for Cu_K by fitting to the ferroelectric instabilities of Cu-doped $KNbO_3$ obtained *ab initio* for 12.5 and 6.25 mol% Cu concentrations. The structure optimizations were performed using the general utility lattice program (GULP).[27] In the shell model, the atoms are represented as pointlike ionic cores and spherical electronic shells. The cores and shells of different atoms interact via the electrostatic Coulomb forces. The shells additionally interact via a two-body Buckingham potential,

$$V_{ij}(r_{ij}) = A_{ij}e^{-r_{ij}/\varrho_{ij}} - \frac{C_{ij}}{r_{ij}^6}, \tag{1}$$

where r_{ij} is the distance between two shells. The core and shell of an atom interact via a spring force,

$$V_{cs} = \frac{1}{2}k_2 r_{cs}^2 + \frac{1}{24}k_4 r_{cs}^4, \tag{2}$$

where r_{cs} is the distance between core and shell. The Buckingham interaction was truncated at a distance of 6.5 Å, the spring interaction at 1 Å.

In order to visualize qualitatively how the Cu substitutionals disturb the arrangement of dipole moments in the surrounding host crystal, we estimated the change in ionic dipole moments of the individual unit cells in a supercell containing Cu substitutionals. While the absolute value of the electric dipole moment of a crystal is not accessible, the change in dipole moment with respect to a reference structure is well defined and measurable.[28] As reference structure we chose the one in which all atoms occupy the lattice sites of the cubic paraelectric (ideal) perovskite structure. In order to determine accurate values for changes in electric dipole moments, both ionic and electronic contributions must be taken into account, e.g., by employing Born effective charges or the Berry-phase approach.[29] To our knowledge, the first attempt to determine the ferroelectric polarization in $KNbO_3$ using the Berry-phase approach was made by Resta *et al.*[30] for the tetragonal phase. Born effective charges of 0.82 (K), 9.13 (Nb), −6.58 (O_1), and −1.68 (O_2, O_3) were obtained, where the O_1-Nb bonds lie along the direction of the polarization, and the O_2-Nb and O_3-Nb bonds are perpendicular to it. A polarization of 35 $\mu C/cm^2$ was found (experiments:[31,32] 30 $\mu C/cm^2$; 37 $\mu C/cm^2$). In $KNbO_3$ and other perovskite oxides, the Born effective charges deviate strongly from the formal ionic ones. Posternak *et al.*[33] attribute the "giant values" of the Born effective charges in $KNbO_3$ to covalent bonding due to hybridization of O $2p$ and Nb $4d$ states. The Born effective charges, which deviate considerably from the formal ones, have the same sign as the formal ones but a larger value, which means that the electronic polarization follows the ionic one. We found that applying Born effective charges obtained in Ref. 34 for the cubic phase of $KNbO_3$ to undoped, ferroelectric $KNbO_3$ enhances the polarization by an almost constant factor of 1.8–1.85 with respect to a calculation with formal charges. In Ref. 34 it is shown that the Born effective charges of $KNbO_3$ depend markedly on the structure. Using the Born effective charge tensor for tetragonal $KNbO_3$ from Ref. 34, the polarization in [001] direction in a cubic unit cell is reduced by 25% compared to the one obtained with Born effective charges for the cubic phase. In principle it is necessary to determine the Born effective charges for each (defect) structure separately. Since we are mainly interested in qualitative effects, we applied a simple approximation using formal ionic charges for calculating changes in ionic dipole moments and neglected the electronic contribution. The change in ionic dipole moment $\Delta\mathbf{P}$ of an individual unit cell is then

$$\Delta\mathbf{P} = e\sum_i w_i Z_i \,\Delta\mathbf{r}_i, \tag{3}$$

where e is the absolute value of the electron charge, Z_i is the nominal charge of ion i, w_i is its weight (e.g., in the B-site centered unit cell in Fig. 1 the weight of the eight A atoms at the corners of the cubic perovskite unit cell is 1/8 because they are shared by eight unit cells), and $\Delta\mathbf{r}_i$ is its distance vector from the reference position. The charges used were K^+, Nb^{5+}, O^{2-}, Cu^+ on K sites, and Cu^{2+} on Nb sites. In the case of Cu, we used the charge states that according to Ref. 10 are energetically most favorable at the center of the band gap. For each unit cell the position of the B site atom was chosen as the reference position.

III. RESULTS

A. Undoped $KNbO_3$

In Table I atomic displacements and the ferroelectric instability of the rhombohedral phase of $KNbO_3$ obtained in

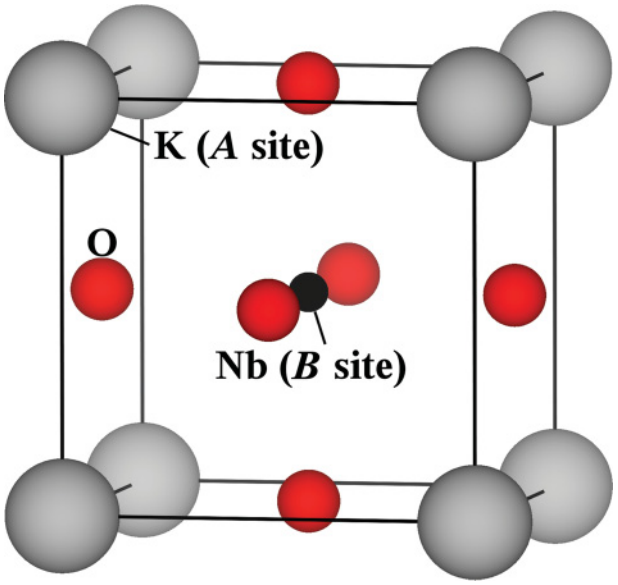

FIG. 1. (Color online) Unit cell of $KNbO_3$ in the ideal cubic perovskite structure.

this work using DFT-LDA are compared to those obtained in Ref. 35, one of the first DFT-LDA studies of $KNbO_3$ using pseudopotentials, and to experiment. Our DFT-LDA setup yields a smaller soft-mode amplitude (smaller ionic displacements) than experiment (by about 1/3 in the case of O), which was also found in Ref. 35. Nevertheless, the ferroelectric instability obtained with the LDA lies close to the experimental one.

The SMP simulations were initiated by means of the SMP of Ref. 36. This potential reproduces the experimental phase transition temperatures very well,[37] but the 0-K total energy differences between ferroelectric structures are overestimated with respect to our DFT results (cf. Table II). Therefore in order to correct for this overestimation of ferroelectric instabilities, the potential parameters were modified as follows: First the Buckingham potential and the spring force constants were multiplied by a factor of 1.016, then the theoretical equilibrium lattice parameter was reduced by rescaling all distances with a factor of 1.0025. The SMP parameters thus obtained and used in this work are compiled in Table III.

In Ref. 38 phonon frequencies of $KNbO_3$ were calculated using the LAPW method and a linear-response approach.

TABLE I. Comparison of the z component (in units of the lattice constant) of the ferroelectric displacements $u_{[111]}$ along [111] and ferroelectric instability in the rhombohedral phase of $KNbO_3$

	DFT-LDA Ref. 35	This work	Expt. Ref. 4
K	0.010[a]	0.008	0.0112
Nb	0.000	0.000	0.0000
$O_{1,2}$	0.019	0.021	0.0295
O_3	0.020	0.021	0.0308
$\Delta E_{[111]}$ (meV)	−10.9[b]	−12.5	−13.3

[a]Obtained from Table VII in Ref. 35.
[b]Obtained from Eq. (20) and Table V in Ref. 35.

TABLE II. Comparison of energies of ferroelectric phases relative to the paraelectric cubic phase (ΔE), c/a ratio, rhombohedral cell angle α, cubic volume V, bulk modulus B, and atomic displacements $u_{[001]}$ of pure tetragonal $KNbO_3$ with a polarization in the $[00\bar{1}]$ direction obtained with the SMP from Ref. 36, the SMP obtained in this work, DFT, and experiment.

	SMP Ref. 36	SMP This work	DFT This work	Expt. Refs. 3, 40, and 41
$\Delta E_{[001]}$ (meV)	−61.6	−9.8	−10.4	−8.2
$\Delta E_{[011]}$ (meV)	−73.3	−11.4	−11.6	−11.9
$\Delta E_{[111]}$ (meV)	−80.4	−12.9	−12.5	−13.3
c/a ([001])	1.042	1.017	1.016	1.017
c/a ([011])	1.029	1.010	1.010	1.017
α (°)	89.34	89.74	89.91	89.83
V (PE, Å^3)	63.57	63.86	61.72	64.04
B (GPa)	199	184	223	165 172
$u_{[001]}$ (K)	0.021	0.016	0.012	0.023
$u_{[001]}$ (Nb)	0.000	0.000	0.000	0.000
$u_{[001]}$ ($O_{1,2}$)	0.061	0.040	0.034	0.042
$u_{[001]}$ (O_3)	0.062	0.037	0.034	0.040

Unstable TO phonon modes were found, indicating that ferroelectric instabilities exist. Table IV contains the phonon frequencies at the Γ point from in Ref. 38, as well as those obtained with our SMP and those measured for the cubic structure at 710 K in Ref. 39. Our SMP gives phonon frequencies that lie similarly close to the experimental ones as the first-principles results from Ref. 38.

Our SMP reproduces the ferroelectric structure and the energy surface of pure $KNbO_3$ as obtained with DFT and from measured heats of formation[3] quite well, if the unit cell parameters are relaxed, although it underestimates the ferroelectric instabilities if the unit cell parameters are fixed to the cubic ones (cf. Fig. 2 and Table II).

B. Cu on K sites

For tetragonal $K_{0.5}Cu_{0.5}NbO_3$, the DFT predicts $c/a = 1.016$, and therefore the same value as in pure $KNbO_3$, whereas the SMP predicts a c/a ratio of 1.044. This finding indicates that our SMP for the Cu-O interaction overestimates strain effects. Because the Cu-O interaction was only fitted to DFT energies of a narrow target range of structures and Cu concentrations, it may not necessarily be widely transferable to arbitrary perovskite phases or high Cu concentrations.

The ferroelectric energy profile of $KNbO_3$ doped with 12.5 and 6.25 mol% Cu_K, respectively, obtained *ab initio* and with the SMP, is shown in Fig. 3. Only the atomic coordinates were allowed to relax; the cell parameters were fixed to the cubic ones in both the DFT and the atomistic calculations.

If Cu_K is added, the ferroelectric instabilities are enhanced, and for 12.5 mol% Cu the relative order of the ferroelectric instabilities is reversed, so that the ground state has no longer rhombohedral ([111]), but tetragonal ([001]) symmetry, resulting in a MPB, at least at low temperatures.

The SMP was used to simulate Cu_K concentrations that are lower than those accessible with DFT in order to determine

TABLE III. SMP parameters [cf. Eqs. (1) and (2)] for Cu-doped $KNbO_3$ obtained and used in this work.

Atom (pair)	A	ϱ	C	Core charge	Shell charge	k_2	k_4
K(−O)	126870.4000	0.194514	0.0	1.237854	−0.418377	229.74443	0.0
Cu(−O)	731.4800	0.282190	0.0	4.944000	−3.777500	767.50000	1215.0378
Nb(−O)	1053.2161	0.389027	0.0	−2.984072	7.816735	255.95572	410.47927
O(−O)	3657.8642	0.282693	200.1785	1.122198	−3.006245	76.581476	1539.2972

the MPB composition at which the ground-state symmetry changes.

Figure 4 shows the energy gain of the tetragonal ([001]), the orthorhombic ([011]), and the rhombohedral ([111]) ferroelectric phases with respect to the paraelectric cubic phase as a function of the Cu content. In the SMP simulation, other than in Fig. 3, both atomic coordinates and cell parameters were allowed to relax. In the DFT calculations, the cell parameters were fixed to the cubic ones. For all three ferroelectric phases the instabilities vary almost linearly with composition. A linear fit was applied using the data for 0, 1.5625, 3.125, and 6.25 mol% Cu content. The SMP predicts a MPB (determined as the crossing point of the linear fits for the tetrahedral and the rhombohedral structure) at a Cu content of 2 mol% (DFT: 4 mol%; SMP with cell parameters fixed to the cubic ones: 3.6 mol%). The orthorhombic phase does not become the ground state for any composition in the range 0–12.5 mol% Cu, but around the MPB composition, the three phases are approximately degenerated in energy.

In order to determine whether the ferroelectric instabilities are more stable than rotational ones, the energy of rotations of the oxygen octahedra around [001] ($R001$, corresponding to $a^0a^0c^+$ and $a^0a^0c^-$ in Glazer's system[42]) and around [111] ($R111$, corresponding to $a^-a^-a^-$) were calculated using DFT and the SMP for the compositions 12.5 and 50 mol% Cu content. These three tilt systems were observed, among others, in other perovskite compounds [$a^0a^0c^+$ in $NaNbO_3$ (T_2 phase), $a^0a^0c^-$ in $SrTiO_3$ (low-temperature phase), and $a^-a^-a^-$ in $NaNbO_3$ (N phase)].[42] The superscripts denote whether the direction of rotation alternates along the corresponding axis (−) or stays the same (+), or if there is no rotation around that axis (0). The results are compiled in Table V, together with those for ferroelectric phases. Other than in Table II, the cell parameters were fixed to the cubic ones in the DFT calculations. In the SMP calculations, they were allowed to relax. Also the monoclinic cell angle of the orthorhombic phase was allowed to deviate from 90°. The SMP predicts a monoclinic angle of 89.65° (experiment:[4] 89.74°). Both DFT and SMP predict the rotational modes to be unstable at 12.5 mol% Cu_K, but stable at 50 mol% Cu_K.

Both DFT and SMP predict the $R111$ mode to be more stable than the $R001$ modes if the lattice parameters are fixed to the cubic ones. The two $R001$ modes have similar energies in both DFT and SMP, but their energetical order comes out oppositely with the two methods. The SMP generally overestimates the energy gain of the rotational modes in $Cu_{0.5}K_{0.5}NbO_3$ by a factor of about 1.5–1.7. If the cell parameters are allowed to relax, the SMP predicts the $R001$ modes to be slightly more stable than the $R111$ mode. In all cases, the rotational modes are less stable than the ferroelectric ones.

Figure 5 shows histograms of the atomic displacements in undoped and Cu_K-doped $KNbO_3$ in a fcc $4 \times 4 \times 4$ supercell (320 atoms). The displacement patterns of the host atoms in the undoped and the doped supercell are very similar, apart from a few K atoms, which are displaced into the opposite direction (with respect to Nb) as in the undoped crystal. The Cu atoms are much more strongly of center than the K atoms (by about 28% of the single unit-cell lattice constant with respect to Nb).

Figure 6 shows the atomic displacements and the change in ionic dipole moment of the individual unit cells obtained by using Eq. (3). In one unit cell, the atomic positions and

TABLE IV. Phonon frequencies in cm^{-1} in $KNbO_3$ from Ref. 38, this work, and experiment (Ref. 39).

Ref. 38	This work	Expt.
TO modes		
147*i*	149*i*	
170	207	198
262	232	280[a]
477	489	521
LO modes		
168	205	190
	232	279[a]
405	360	419
743	835	826

[a]Measured in the tetragonal structure at 585 K.

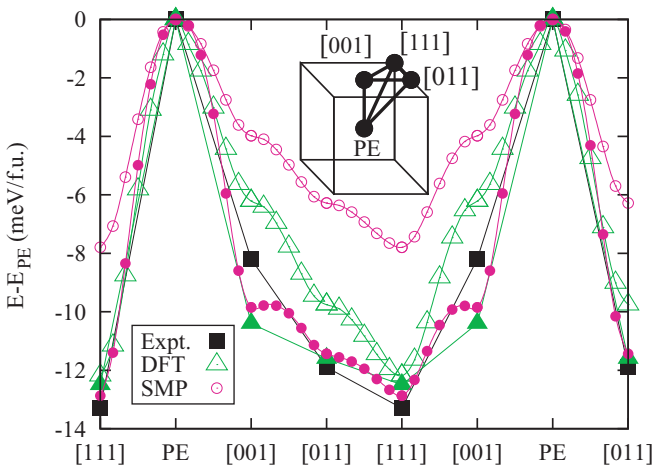

FIG. 2. (Color online) Energy profile in meV per perovskite formula unit along linear transitions between the different polarization directions (see inset; PE: paraelectric cubic perovskite structure) in pure $KNbO_3$. Black squares: experiment; green triangles: DFT; red circles: SMP. Open symbols: unit-cell parameters fixed to the cubic ones; filled symbols: relaxed unit-cell parameters. The lines serve as a guide to the eye.

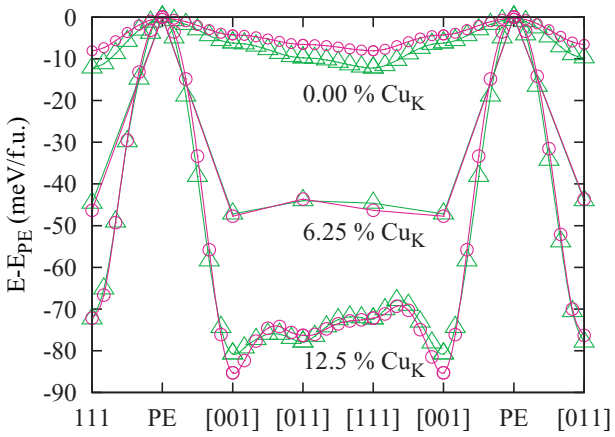

FIG. 3. (Color online) The energy profile obtained *ab initio* and with the SMP for cubic supercells of pure (top) and Cu_K-doped $KNbO_3$. Green triangles: DFT; red circles: SMP. The curves for undoped $KNbO_3$ are the same as in Fig. 2.

displacements are drawn as well for a perfect reference cell (ΔP_r denotes the change in ionic dipole moment of a perfect unit cell). The arrangement of dipole moments looks similar to that of the undoped crystal (shaded cell).

C. Cu on Nb sites

Figure 7 shows the ferroelectric instabilities obtained *ab initio* for undoped $KNbO_3$ and for $KNbO_3$ doped with 6.25% and 12.5% Cu on Nb sites, respectively. At a doping level of 6.25%, the ferroelectric energy differences are reduced compared to the undoped material at both the unrelaxed and the relaxed volume. For 12.5 mol% Cu_{Nb} the ferroelectric instabilities are reduced to almost zero, if the volume is fixed to that of the undoped material. If volume relaxation is taken into account, an overall increase of the volume by about 2% takes place, and the ferroelectric instabilities are larger than in the undoped material. The inset shows the ferroelectric energy gain in undoped $KNbO_3$ as a function of the lattice constant. The vertical lines denote the equilibrium lattice constant of undoped $KNbO_3$ and those of $KNbO_3$ doped with 6.26 and 12.5 mol% Cu_{Nb}, respectively.

Figure 8 shows histograms of the ferroelectric displacements in $KNbO_3$ doped with 6.25 mol% Cu_{Nb}, and in the undoped $KNbO_3$. Although the displacement pattern

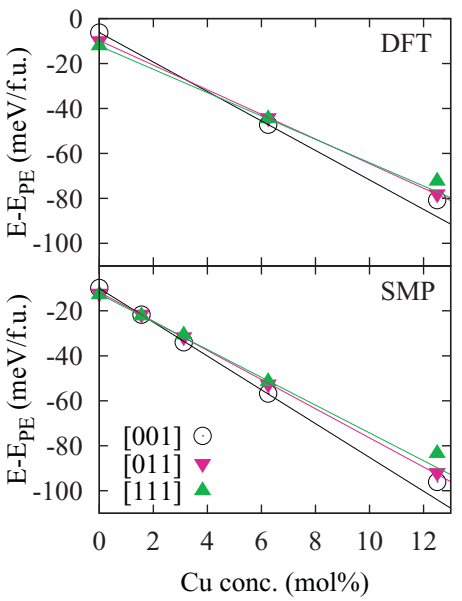

FIG. 4. (Color online) [001], [011], and [111] instabilities in meV per perovskite formula unit relative to the cubic, paraelectric phase as a function of the Cu content in mol% obtained with DFT (top) and the SMP (bottom).

qualitatively follows that of the undoped material, the numbers scatter strongly (more than for Cu_K doping, cf. Fig. 5). Cu is hardly shifted off center at all, and the averaged displacements are smaller than in the undoped bulk.

Figure 9 shows the atomic positions, displacements, and change in ionic dipole moment [cf. Eq. (3)] for each unit cell in a supercell that contains 6.25 mol% Cu_{Nb} and is polarized along the $[00\bar{1}]$ direction (cf. Fig. 6).

IV. DISCUSSION

A. Cu on K sites

Since the SMP underestimates the ferroelectric instabilities without strain (cf. Fig. 2), it may underestimate the Cu content at the MPB composition as well. Therefore the 2 mol% obtained in this work using the SMP should be regarded as a lower barrier. An upper barrier is the DFT prediction for unit-cell parameters fixed to the cubic ones (4 mol%). At finite temperatures, the MPB may shift further.

TABLE V. Energies of the [001], [011], [111], $R001$ ($a^0a^0c^+$ and $a^0a^0c^-$), and $R111$ ($a^-a^-a^-$) instabilities with respect to the cubic paraelectric phase in meV per perovskite formula unit as a function of the Cu concentration in % obtained with DFT and our SMP. f: cell parameters fixed to the cubic ones; r: relaxed cell parameters.

	[001]		[011]		[111]		$a^0a^0c^+$			$a^0a^0c^-$			$a^-a^-a^-$		
Cu	DFT	SMP	DFT	SMP	DFT	SMP	DFT	SMP	SMP	DFT	SMP	SMP	DFT	SMP	SMP
Conc. (%)	f	r	f	r	f	r	f	f	r	f	f	r	f	f	r
0.0	−6.2	−9.8	−9.8	−12.1	−12.2	−12.9									
1.5625		−21.7		−21.5		−22.3									
3.125		−34.0		−31.5		−30.8									
6.25	−55.5	−56.8	−51.7	−52.5	−52.5	−51.6									
12.5	−80.8	−96.1	−77.9	−91.9	−72.4	−83.5	0.0	0.0	0.0	0.0	0.0	0.0	0.0	0.0	0.0
50.0	−317.0	−491.3		−313.9		−448.8	−30.3	−46.1	−104.2	−28.5	−49.7	−108.9	−35.5	−56.2	−97.0

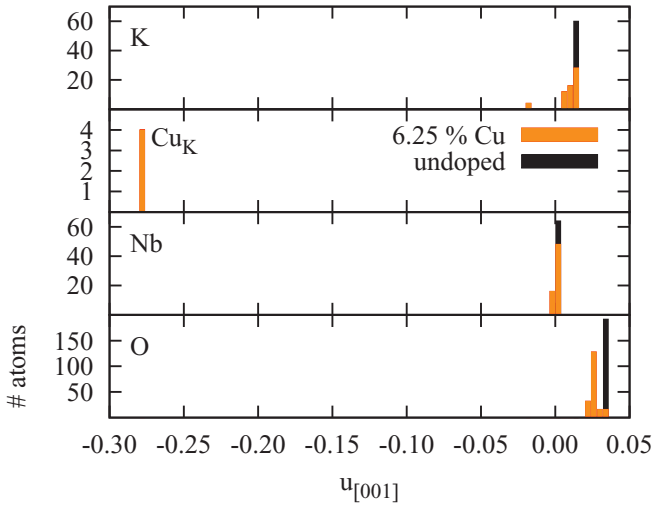

FIG. 5. (Color online) Atomic displacements $u_{[001]}$, in units of the lattice constant of a single $KNbO_3$ unit cell, with respect to the paraelectric positions for all unit cells in a supercell polarized in the [00$\bar{1}$] direction for undoped $KNbO_3$ and 6.25 mol% Cu_K doping. The averaged Nb displacement was set to zero.

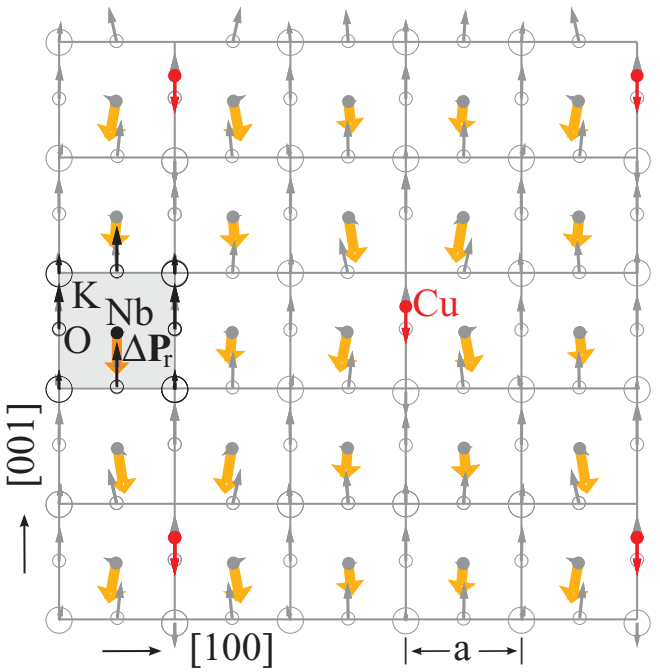

FIG. 6. (Color online) Atomic displacements in the (010) plane (thin gray and red arrows) and change in ionic dipole moment (bold orange arrows) of the unit cells in a supercell which contains 6.25 mol% Cu_K and is polarized in the [00$\bar{1}$] direction. The arrows that mark the displacements of K, Nb, and O (all except for those of Cu) are scaled by a factor of 10 for better visibility. Black circles, small black arrows, and the bold orange arrow in the shaded cell on the left mark the atom positions, displacements, and change in ionic dipole moment $\Delta\mathbf{P}_r$ of a perfect reference cell, respectively.

In an earlier atomistic study of the instabilities for the [001], [011], and [111] displacements of an isolated Li_K dopant in $KTaO_3$ by Exner *et al.*,[43] the same energetical ordering ([111] → [011] → [001]) was found as in the present work for Cu_K. The tetragonal instability of the hypothetical composition $K_{0.5}Cu_{0.5}NbO_3$ found with the DFT is 317 meV (SMP: 491 meV, cf. Table V), which is a similar value as the 222 meV found in Ref. 8 for $K_{0.5}Li_{0.5}NbO_3$. The very large off-center displacements of Cu_K obtained in this work were also found by Bilc and Singh for Li_K (from Fig. 2 in Ref. 8 we estimate about 23% of a single perovskite lattice constant with respect to Nb). These findings support the similarity of the effects of Li and Cu doping on K sites in $KNbO_3$. In spite of the large off-center displacements of Cu_K the arrangement of dipole moments is similar to that of the bulk even in the cells that contain the Cu dopants.

Analogous to the shallow instability of ≈12 meV found for the octahedral rotation around [001] and [111] in Ref. 8 for $Li_{0.5}K_{0.5}NbO_3$, in the present work we obtained an energy gain of 30.3 meV per formula unit for the rotation around [001] and 35.5 meV for the rotation around [111], in $Cu_{0.5}K_{0.5}NbO_3$, which are both much smaller than the 317 meV of the ferroelectric displacements in the [001] direction.

Due to competing incorporation of Cu on Nb sites[10] and second phase formation[44] the MPB may be difficult to obtain. Another drawback may be the semiconduction found for $CuNbO_3$,[16] which might limit the ferroelectric performance also in the solid solution. On the other hand, in Ref. 10 we found that a reducing processing atmosphere should drive Cu to the K sites, and that the most stable charge state is Cu_K^+ for a large range of electronic chemical potentials. In this case no free charge carriers are generated.

B. Cu on Nb sites

Cu on Nb sites causes two opposite effects: an increase of the ferroelectric energy gain at high (unrealistic) doping levels (e.g., 12.5%), and a decrease of the ferroelectric energies at lower doping levels (e.g., 6.25%). In both 40-atom and 80-atom supercells, in all individual unit cells the change in ionic dipole moment is smaller than in the undoped bulk cells. A plausible explanation for these findings is the following: The larger ionic radius of Cu^{2+} as compared to Nb^{5+} (0.73 vs 0.64 Å) (Ref. 13) leads to an overall volume increase. Because the ferroelectric energy is extremely sensitive to volume changes, the ferroelectric energy of the expanded cell can increase. The inset in Fig. 7 shows the increase in ferroelectric energy gain as function of the lattice constant in an undoped $KNbO_3$ unit cell. A cubic unit cell was imposed. Increasing the lattice constant of undoped $KNbO_3$ by 2% (like in the case of 12.5 mol% Cu doping) with respect to the optimum one increases the ferroelectric energy gain by a factor of about 5.6. Increasing the lattice constant by 0.8%, like in the case of 6.25 mol% Cu doping, increases the ferroelectric instability by the much smaller factor of about 2.3. The increase of the lattice constant with the Cu doping level is only weakly nonlinear, but the ferroelectric instability increases with the lattice constant in a strongly nonlinear way. On the other hand, the smaller change in ionic dipole moments of the individual cells in $KNbO_3$ doped with Cu_{Nb} reduces the ferroelectric energy gain. In the 40-atom cell, the volume effect overcompensates for the reduced change in ionic dipole moments, so that the ferroelectric energy gain increases. In the 80-atom cell, the volume effect is less strong and cannot

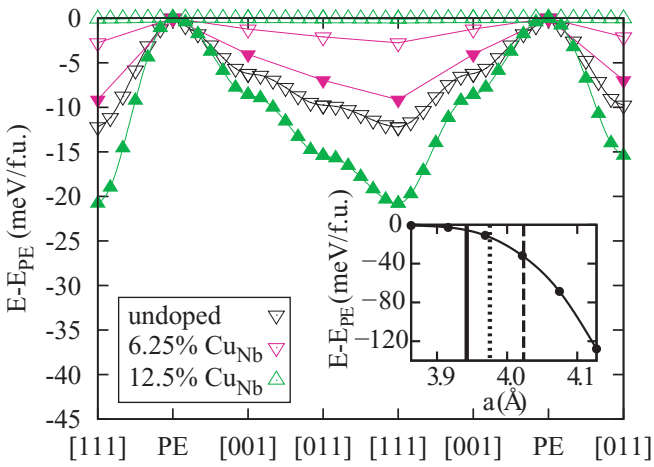

FIG. 7. (Color online) The energy profile as in Fig. 3, but for Cu on Nb sites, and only DFT results are shown. Filled symbols: relaxed volume; open symbols: volume fixed to the cubic volume of the undoped material. Inset: energy gain due to atomic displacements in the [001] direction for undoped $KNbO_3$ as a function of the lattice constant. Vertical lines denote the equilibrium lattice constant for undoped $KNbO_3$ (solid line), 6.25 mol% Cu (dotted line), and 12.5 mol% Cu (dashed line).

compensate for the reduced change in ionic dipole moment, so that the ferroelectric energy gain is smaller than in the undoped bulk.

The isolated Cu_{Nb} dopants strongly disturb the arrangement of dipole moments of the surrounding bulk region. In the 80-atom supercell containing one Cu atom, in all unit cells the atomic displacements are quite different from those in the pure crystal. This finding can be attributed to the rather shallow ferroelectric instability in $KNbO_3$ as compared to, e.g., $PbTiO_3$ [we obtained 11 meV/f.u. in tetragonal $KNbO_3$ as compared to 53 meV/f.u. in tetragonal $PbTiO_3$ (Ref. 45)], so that the atomic structure can be strongly influenced by lattice defects.

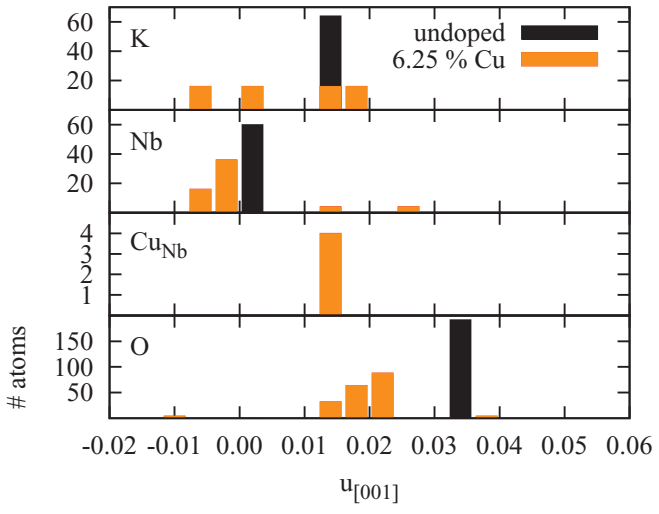

FIG. 8. (Color online) The same as Fig. 5 for Cu_{Nb} doping. Note the change of scale.

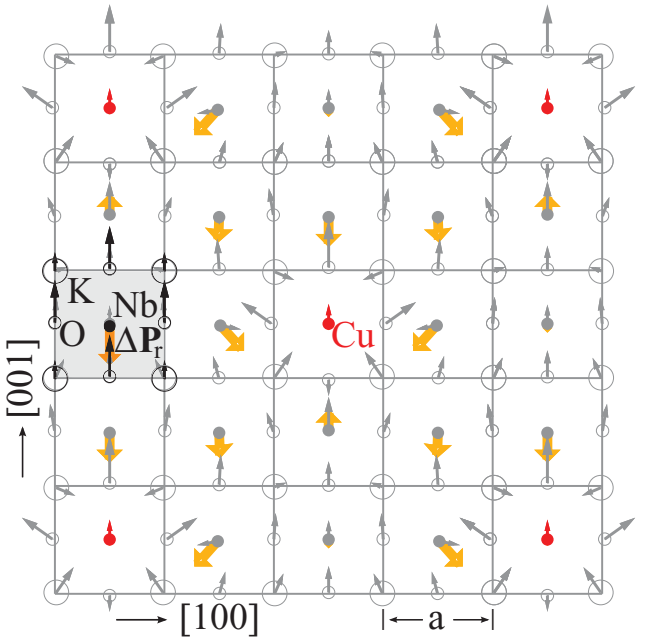

FIG. 9. (Color online) The same as Fig. 6 for 6.25 mol% Cu_{Nb}. The arrows that mark the displacements, including those of Cu, are scaled by a factor of 10.

However, isolated Cu_{Nb} substitutionals will be rather an exception because of the large charge difference between Nb and Cu, and the effects of defect complexes of Cu and oxygen vacancies are likely much stronger than those of a small concentration of isolated Cu_{Nb} substitutionals and hence determine the overall ferroelectric behavior of the material.

V. CONCLUSION

On the basis of *ab initio* DFT calculations an empirical atomistic shell-model potential for the Cu-O interaction in Cu_K-doped $KNbO_3$ was obtained. DFT and the shell-model potential predict a morphotropic phase boundary between the rhombohedral ground state of $KNbO_3$ and a tetragonal structure at about 2–4 mol% Cu_K at low temperatures, analoguous to Li_K. Regarding the structural properties, the effect of Cu_K doping is very similar to that of Li_K. If Cu is driven to the alkali sites, e.g., by processing in a reducing atmosphere, a Cu doping level of a few percent could, besides improving the sinterability, enhance the piezoelectric properties of $KNbO_3$ or KNN due to the MPB. Isolated Cu dopants on Nb sites reduce the ferroelectric instabilities but do not change their energetical order and therefore do not give rise to a MPB.

ACKNOWLEDGMENTS

Financial funding by the German Research Foundation (DFG, Grant No. EL 155/21-1,2), computer resources at the Karlsruhe Institute of Technology, Germany (KIT), and helpful discussions with Pierre Hirel about electric polarization in crystals are gratefully acknowledged. The perovskite structure was visualized with VESTA.[46]

*sabine.koerbel@iwm.fraunhofer.de

[1] S. Zhang, R. Xia, and T. R. Shrout, J. Electroceram. **19**, 251 (2007).
[2] Y. Guo, K. Kakimoto, and H. Ohsato, Appl. Phys. Lett. **85**, 4121 (2004).
[3] G. Shirane, H. Danner, A. Pavlovic, and R. Pepinski, Phys. Rev. **93**, 672 (1954).
[4] A. W. Hewat, J. Phys. C **6**, 2559 (1973).
[5] G. Shirane, R. Newnham, and R. Pepinsky, Phys. Rev. **96**, 581 (1954).
[6] S. C. Abrahams, W. C. Hamilton, and J. M. Reddy, J. Phys. Chem. Solids **27**, 1013 (1966).
[7] H. D. Megaw, Acta Crystallogr., Sect. A **24**, 583 (1968).
[8] D. I. Bilc and D. J. Singh, Phys. Rev. Lett. **96**, 147602 (2006).
[9] M. Matsubara, K. Kikuta, and S. Hirano, J. Appl. Phys. **97**, 114105 (2005).
[10] S. Körbel, P. Marton, and C. Elsässer, Phys. Rev. B **81**, 174115 (2010).
[11] E. Erünal, R.-A. Eichel, S. Körbel, C. Elsässer, J. Acker, H. Kungl, and M. J. Hoffmann, Functional Materials Letters **3**, 19 (2010).
[12] Dunmin Lin, K. W. Kwok, and H. L. W. Chan, Appl. Phys. Lett. **90**, 232903 (2007).
[13] R. D. Shannon, Acta Crystallogr., Sect. A **32**, 751 (1976).
[14] M. Paul, A. V. Chadwick, and A. R. West, J. Mater. Chem. **5**, 1043 (1995).
[15] B. O. Marinder and E. Wahlstroem, Chem. Scr. **23**, 157 (1984).
[16] A. W. Sleight and C. T. Prewitt, Mater. Res. Bull. **5**, 207 (1970).
[17] I. Grinberg and A. M. Rappe, Appl. Phys. Lett. **85**, 1760 (2004).
[18] C. Elsässer, N. Takeuchi, K. Ho, C. Chan, P. Braun, and M. Fähnle, J. Phys.: Condens. Matter **2**, 4371 (1990).
[19] K. Ho, C. Elsässer, C. Chan, and M. Fähnle, J. Phys.: Condens. Matter **4**, 5189 (1992).
[20] B. Meyer, K. Hummler, C. Elsässer, and M. Fähnle, J. Phys.: Condens. Matter **7**, 9201 (1995).
[21] F. Lechermann, F. Welsch, C. Elsässer, C. Ederer, M. Fähnle, J. M. Sanchez, and B. Meyer, Phys. Rev. B **65**, 132104 (2002).
[22] B. Meyer, F. Lechermann, C. Elsässer, and M. Fähnle, *Fortran90 Program for Mixed-Basis Pseudopotential Calculations for Crystals* (unpublished).
[23] D. Vanderbilt, Phys. Rev. B **32**, 8412 (1985).
[24] J. P. Perdew and A. Zunger, Phys. Rev. B **23**, 5048 (1981).
[25] D. J. Chadi and M. L. Cohen, Phys. Rev. B **8**, 5747 (1973).
[26] C. L. Fu and K. M. Ho, Phys. Rev. B **28**, 5480 (1983).
[27] J. D. Gale and A. L. Rohl, Mol. Simul. **29**, 291 (2003).
[28] R. Resta, Ferroelectrics **136**, 51 (1992).
[29] M. V. Berry, Proc. R. Soc. London, Ser. A **392**, 45 (1984).
[30] R. Resta, M. Posternak, and A. Baldereschi, Phys. Rev. Lett. **70**, 1010 (1993).
[31] S. Triebwasser, Phys. Rev. **101**, 993 (1956).
[32] W. Kleemann, F. J. Schäfer, and M. D. Fontana, Phys. Rev. B **30**, 1148 (1984).
[33] M. Posternak, R. Resta, and A. Baldereschi, Phys. Rev. B **50**, 8911 (1994).
[34] C.-Z. Wang, R. Yu, and H. Krakauer, Phys. Rev. B **54**, 11161 (1996).
[35] R. D. King-Smith and D. Vanderbilt, Phys. Rev. B **49**, 5828 (1994).
[36] Sepliarsky, A. Astaghiri, S. R. Phillpot, M. G. Stachiotti, and R. L. Migoni, Curr. Opin. Solid State Mater. Sci. **9**, 107 (2005).
[37] S. Tinte, M. Sepliarsky, M. G. Stachiotti, R. L. Migoni, and C. O. Rodriguez, Z. Phys. B **104**, 721 (1997).
[38] R. Yu and H. Krakauer, Phys. Rev. Lett. **74**, 4067 (1995).
[39] M. D. Fontana, G. M'etrat, J. L. Servoin, and F. Gervais, J. Phys. C **17**, 483 (1984).
[40] A. W. Hewat, J. Phys. C **6**, 1074 (1973).
[41] J. C. Chervin, J. P. Itié, D. Gourdain, and Ph. Pruzan, Solid State Commun. **110**, 247 (1999).
[42] A. M. Glazer, Acta Crystallogr., Sect. B **28**, 3384 (1972).
[43] M. Exner, C. R. A. Catlow, H. Donnerberg, and O. F. Schirmert, J. Phys.: Condens. Matter **6**, 3379 (1994).
[44] M. Matsubara, T. Yamaguchi, W. Sakamoto, K. Kikuta, T. Yogo, and S. I. Hirano, J. Am. Ceram. Soc. **88**, 1190 (2005).
[45] Y. Umeno, B. Meyer, C. Elsässer, and P. Gumbsch, Phys. Rev. B **74**, 060101 (2006).
[46] K. Momma and F. Izumi, J. Appl. Crystallogr. **41**, 653 (2008).